

Arbitrary high-fidelity binomial codes from multiphoton spin-boson interactions

Pradip Laha^{1,*} and Peter van Loock^{1,†}

¹*Institute of Physics, Johannes Gutenberg-Universität Mainz, Staudingerweg 7, 55128 Mainz, Germany*

Encoding a qubit in the continuous degrees of freedom of a quantum system, such as bosonic modes, is a powerful alternative to modern quantum error correction (QEC). Among the most prominent bosonic QEC codes, binomial codes provide protection against loss and dephasing errors by encoding logical states in superpositions of Fock states with binomially weighted coefficients. While much attention has been given to their error-correcting capabilities and integration into fault-tolerant architectures, efficient methods for generating arbitrary binomial codewords remain scarce. In this work, we propose a novel scheme for generating these codewords by exploiting nonlinear multiphoton interactions between a continuous-variable bosonic mode (oscillator) and a two-level system (spin/qubit). Our proposed scheme assumes the ability to prepare the oscillator in an arbitrary Fock state and the qubit in an arbitrary superposition of its basis states and access to arbitrarily high multiphoton interactions. To enhance the experimental feasibility of our scheme, we further demonstrate how to reduce the required order parameter of multiphoton interactions by a factor of two for a special class of code states.

I. INTRODUCTION

Quantum error correction (QEC) plays a foundational role in enabling scalable quantum information processing, providing a systematic framework to safeguard fragile quantum states from decoherence and other operational noise [1–5]. While conventional QEC schemes typically encode logical information into discrete-variable (DV) qubit registers, continuous-variable (CV) approaches leverage the infinite-dimensional Hilbert space structure of bosonic modes (or qumodes, such as quantized electromagnetic fields) to encode and protect quantum information [6–8]. Owing to their intrinsic redundancy and potential for resource-efficient error mitigation [9], CV-based error correction has attracted growing interest, making bosonic codes particularly promising for near-term quantum hardware where qubit resources are limited and noise is prevalent [10–22]. Prominent examples of encoding a qubit in bosonic modes include Gottesman-Kitaev-Preskill (GKP) codes [23–28], which protect against small displacement errors, and cat codes [29–34], which leverage coherent state superpositions to mitigate photon loss. These code states have demonstrated remarkable potential in experimental platforms such as superconducting circuits [12, 35–37], optical systems [38–40], and trapped ions [11, 18, 41].

Alongside these, binomial encoding [42] has emerged as a compelling alternative, offering protection against both photon loss and dephasing errors while requiring only modest hardware overhead [43]. These codes encode quantum information into superpositions of Fock states with binomially weighted amplitudes, carefully designed so that common error processes map codewords onto orthogonal, correctable states. Their discrete structure, analytical tractability, and compatibility with bosonic

modes make them highly attractive for near-term quantum technologies [12, 22, 44–50]. Binomial codes have been explored across a range of physical architectures, including superconducting circuits [12, 45, 47], light-matter systems [44], and trapped ions [11]. Recent studies have evaluated the fault tolerance and scalability of binomial codes under realistic noise [51]. Ref. [48] examined concatenated architectures and identified photon-loss thresholds for different measurement strategies, while Ref. [52] proposes a scheme for logical qubit rotations within the binomial code space without the need for an ancillary qubit. Further, a quantum repeater architecture based on binomial codes has been proposed, employing a microwave cavity and a superconducting transmon to suppress photon loss while enabling high-fidelity state preparation and entanglement swapping [53]. In parallel, high-fidelity preparation of binomial code states has been experimentally demonstrated in a circuit-QED architecture by employing transmon-mediated sideband interactions, enabling efficient multimode control and state encoding [54].

Despite significant progress, the high-fidelity generation of *arbitrary* binomial codewords remains a critical challenge. Most recent efforts to date have primarily focused on the simplest instance—protection against a single photon loss—where the two logical states of the qubit are given by $|\bar{0}\rangle = (|0\rangle + |4\rangle)/\sqrt{2}$ and $|\bar{1}\rangle = |2\rangle$, respectively. Here, $|n\rangle$ is an n -photon Fock state ($n = 0, 2, 4$). However, the general binomial code framework introduced in Ref. [43] enables protection against multiple photon loss, gain, and dephasing errors, albeit with increasingly complex logical encodings. Developing a universal, hardware-independent protocol for the high-fidelity preparation of arbitrary binomial codewords would mark a major step toward scalable, modular quantum architectures based on bosonic encodings.

In this work, we address this gap by introducing a novel protocol based on the multiphoton Jaynes–Cummings (MPJC) interaction, a highly nonlinear coupling between a two-level system (spin/qubit) and a bosonic mode. Ini-

* plaha@uni-mainz.de

† loock@uni-mainz.de

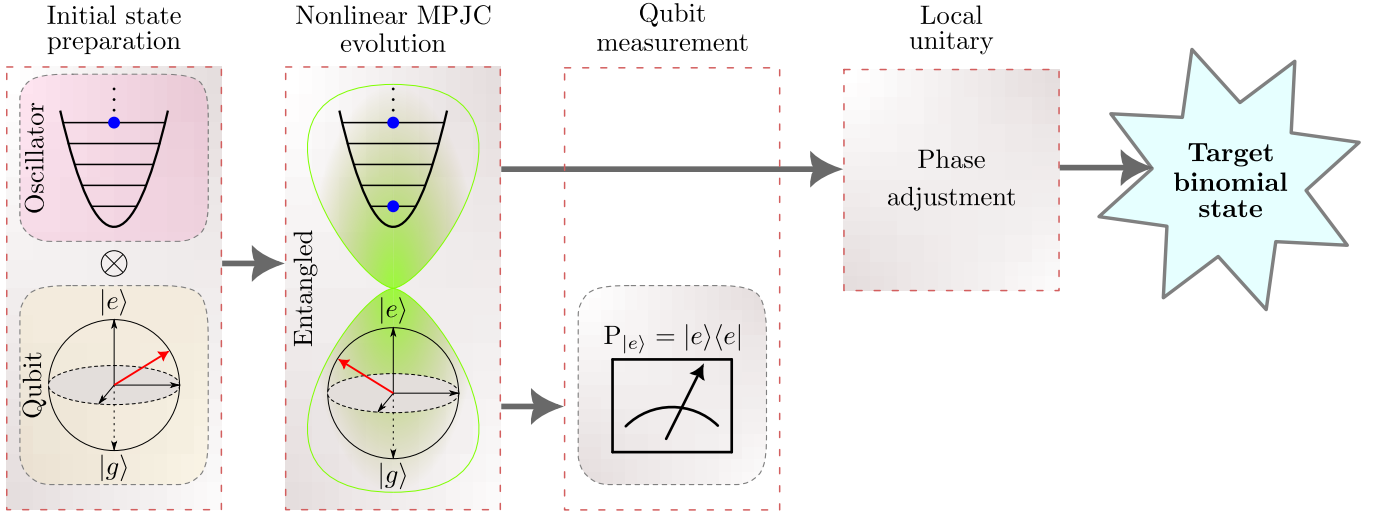


Figure 1. Schematic of the proposed protocol for synthesizing binomial code states composed of two Fock state superpositions. The protocol begins with state preparation, where the oscillator is initialized in a Fock state $|n_1\rangle$ (black solid circle) and the qubit in a superposition state $\cos \theta |g\rangle + \sin \theta |e\rangle$ (red arrow). The joint system then undergoes an entangling evolution governed by a nonlinear multiphoton Jaynes–Cummings (MPJC) interaction of order m , mediated by a tunable coupling strength g . A projective measurement on the qubit at an optimized interaction time τ collapses the oscillator into a nontrivial superposition of Fock states. A final local unitary operation on the oscillator corrects the relative phase and completes the synthesis of the desired binomial code state. The parameters n_1 , m , θ , and τ uniquely determine the final encoded state. The protocol can be recursively applied to construct more complex binomial states involving additional Fock components (see main text).

tially developed in the context of nonlinear optics and cavity quantum electrodynamics (QED) [55–59], MPJC-type Hamiltonians have seen renewed interest [60–64] due to their increasing experimental accessibility in quantum platforms such as superconducting circuits [65, 66] and trapped ions [67, 68].

Our approach exploits the nonlinearities inherent in the multiphoton generalization of the standard Jaynes–Cummings (JC) interaction to coherently drive the oscillator into arbitrary binomial codewords during its time evolution with high fidelity. Note that the standard JC interaction as directly available in cavity QED, including its dispersive regimes enabling spin-controlled phase rotations of an oscillator mode, has been shown [69] to be applicable for both cat code state engineering and cat code photon loss error syndrome identification. For the former, standard cavity QED interactions can be employed in an iterative fashion, starting from a *primitive state* [14]. It is tempting to consider a similar iterative approach to the generation of binomial code states. However, while the primitive state for the cat code is a simple coherent state, the primitive states associated with the binomial code are, from an experimental point of view, not really easier to realize than the target codewords themselves (see Appendix C for a brief discussion on this).

To achieve our objective, we assume initialization of the oscillator in a known Fock state and the qubit in an arbitrary superposition of its two basis states and access to tunable multiphoton interactions of arbitrary order. Under these conditions, and with appropriate local unitaries, we demonstrate high-fidelity synthesis of any bi-

nomial codeword (see Fig. 1). While our primary focus is on the probabilistic protocol—based on postselected qubit measurements—owing to its enhanced flexibility in parameter selection and higher achievable fidelities, we also demonstrate that similar target states can be synthesized deterministically by tracing out the qubit, albeit with a modest reduction in fidelity due to the mixedness introduced by this operation. Both analytical and numerical results confirm the scalability of our protocol to increasingly complex logical states.

While arbitrary oscillator Fock state preparation is now feasible across many quantum platforms [70–77], it is crucial to note that neither the standard nor multiphoton JC interactions can generate subsystem coherence from an initially incoherent joint state [59, 63, 78]. In our protocol, coherence in the spin state is therefore essential, as it seeds the coherence required in the initially incoherent oscillator state. Optimizing this initial spin coherence is consequently key to synthesizing the target bosonic state in a single step with high fidelity. A practical challenge in multiphoton protocols is the scaling of the required multiphoton order parameter with increasing code distance. To improve feasibility, we propose a two-step implementation that reduces the necessary photon-number requirement by a factor of two. This one-time improvement is achieved through judicious choices of initial conditions and by leveraging symmetries in the MPJC dynamics. Finally, to analyze the robustness of our scheme in realistic settings, we also briefly discuss the role of inevitable environmental-induced effects, including oscillator damping and qubit dephasing.

The remainder of this paper is organized as follows.

Section II provides an overview of the structure and properties of binomial codes. In Sec. III, we introduce the MPJC Hamiltonian and describe the theoretical framework of our state-generation protocol. Sections IV and V present explicit constructions of binomial codewords involving two and three Fock components, respectively, using a probabilistic scheme. In Sec. VI, we examine how the required multiphoton parameter can be reduced, improving experimental feasibility. Section VII analyzes the impact of decoherence due to system–environment coupling on the fidelity of the generated states. We conclude in Sec. VIII with a brief summary and outlook. Supplementary technical details and extended results, including those pertaining to the deterministic generation protocol, are provided in the appendices.

II. BINOMIAL CODE STATES

As noted earlier, the generic binomial code encodes the two logical qubit states into superpositions of Fock states with binomially distributed amplitudes. It was first introduced in Ref. [43] as a two-parameter (N, S) code space to correct against up to L photon losses, up to G photon gain errors, and D dephasing events. Here, $S = L + G$ decides the spacing of the superpositions of Fock states, and $N = \max\{L, G, 2D\}$ is responsible for the number of Fock states that are present in the superposition. The generic class of the two logical states is defined as

$$|\bar{\mu}\rangle_{N,S} = \frac{1}{\sqrt{2^N}} \sum_{k=0}^{\lceil \frac{N+1}{2} \rceil - \mu} \sqrt{\binom{N+1}{2k+\mu}} |(S+1)(2k+\mu)\rangle, \quad (1)$$

where, $\mu = 0, 1$, and $\lceil \cdot \rceil$ denotes the ceiling function [48]. For simplicity, we neglect photon gain errors in this work (i.e., $G = 0$), such that $S = L$ and $N = \max\{L, 2D\}$. For a fixed value of L , the number of correctable dephasing errors is determined by N . In the asymptotic limit $N \rightarrow \infty$, the binomial codes asymptotically approach the $2(L+1)$ -legged cat codes [30–33], which are known to protect against up to L photon loss errors, as discussed in Ref. [43]. Both binomial and cat codes belong to the broader class of rotation-symmetric bosonic codes (RBSCs) [14, 51, 79], characterized by their invariance under discrete rotations by a fixed angle in phase space. We now illustrate several explicit examples of binomially encoded logical qubit states.

The simplest and most well-known instance—mentioned in the previous section—corresponds to the case $S = 1$, which corrects a single photon loss. The associated logical states are $|\bar{0}\rangle_{1,1} = \frac{1}{\sqrt{2}}(|0\rangle + |4\rangle)$, and $|\bar{1}\rangle_{1,1} = |2\rangle$, where $N = 1$. By fixing $S = 1$ and increasing N , one obtains codewords that maintain protection against single photon loss while improving resilience to dephasing. Examples of such higher-order

encodings are

$$|\bar{0}\rangle_{2,1} = \frac{1}{2}(|0\rangle + \sqrt{3}|4\rangle), \quad (2a)$$

$$|\bar{1}\rangle_{2,1} = \frac{1}{2}(\sqrt{3}|2\rangle + |6\rangle), \quad (2b)$$

$$|\bar{0}\rangle_{3,1} = \frac{1}{2\sqrt{2}}(|0\rangle + \sqrt{6}|4\rangle + |8\rangle), \quad (2c)$$

$$|\bar{1}\rangle_{3,1} = \frac{1}{\sqrt{2}}(|2\rangle + |6\rangle), \quad (2d)$$

$$|\bar{0}\rangle_{4,1} = \frac{1}{4}(|0\rangle + \sqrt{10}|4\rangle + \sqrt{5}|8\rangle), \quad (2e)$$

$$|\bar{1}\rangle_{4,1} = \frac{1}{4}(\sqrt{5}|2\rangle + \sqrt{10}|6\rangle + |10\rangle), \quad (2f)$$

$$|\bar{0}\rangle_{5,1} = \frac{1}{4\sqrt{2}}(|0\rangle + \sqrt{15}|4\rangle + \sqrt{15}|8\rangle + |12\rangle), \quad (2g)$$

$$|\bar{1}\rangle_{5,1} = \frac{1}{4\sqrt{2}}(\sqrt{6}|2\rangle + \sqrt{20}|6\rangle + \sqrt{6}|10\rangle). \quad (2h)$$

On the other hand, the lowest-order binomial codewords capable of correcting up to two photon loss events ($S = 2$) are

$$|\bar{0}\rangle_{2,2} = \frac{1}{2}(|0\rangle + \sqrt{3}|6\rangle), \quad (3a)$$

$$|\bar{1}\rangle_{2,2} = \frac{1}{2}(\sqrt{3}|3\rangle + |9\rangle). \quad (3b)$$

Higher-order encoded states corresponding to larger S and N values can be systematically constructed from Eq. (1). The objective of this work is to produce arbitrary superpositions of these Fock states with high fidelity.

III. MULTIPHOTON SPIN-BOSON HAMILTONIAN

The JC model [80, 81] captures the fundamental physics of light–matter interactions and forms the basis for understanding cavity and circuit QED systems. It plays a central role in the theoretical and experimental development of quantum optics and quantum information platforms [82]. The standard JC model describes the coherent coupling between a two-level system (spin) and a single quantized harmonic oscillator mode (boson). The two states of the qubit, $|g\rangle$ and $|e\rangle$, are assumed to be separated by a transition frequency ω_0 , while the oscillator is characterized by respective bosonic creation and annihilation operators a^\dagger and a , with mode frequency ω . The detuning is typically denoted as $\Delta = \omega_0 - \omega$. The free energy Hamiltonian is expressed as $H_0 = \frac{\omega_0}{2}\sigma_z + \omega a^\dagger a$ while the interaction Hamiltonian in the limit $\Delta = 0$ (on resonance) is given by $H_{\text{int}} = g(a\sigma_+ + a^\dagger\sigma_-)$ where g denotes the strength of the spin-boson interaction. Here, $\sigma_z = |e\rangle\langle e| - |g\rangle\langle g|$, $\sigma_+ = |e\rangle\langle g|$, $\sigma_- = |g\rangle\langle e|$ are the standard spin operators.

Over the years, the standard JC model has been extended in various directions to capture richer quantum phenomena (see Ref. [82] for a review). Among these, the multiphoton generalization is particularly notable [55–58, 60]. The MPJC model describes a coherent exchange

of m bosonic excitations with a two-level system. Its interaction Hamiltonian is given by

$$H_{\text{int}} = g(a^m \sigma_+ + a^{\dagger m} \sigma_-), \quad (4)$$

where m is the multiphoton order parameter and g is the effective coupling strength. The case $m = 1$ recovers the standard JC model. In what follows, we will find out that m plays a crucial role in engineering the desired quantum superposition states. We mention in passing a recent circuit QED demonstration of single-mode control over cavity modes by preparing both Fock states $|n\rangle$ and vacuum–Fock superpositions $(|0\rangle + |n\rangle)/\sqrt{2}$ by climbing the JC ladder with transmon rotations and sideband pulses. Fock states are prepared using a sequence of broadband pulses followed by sideband π pulses. Consequently, a novel shelving method is employed to achieve superposition states [54].

A. Time-evolved state of the MPJC Hamiltonian

Before proceeding, we summarize the key assumptions of our state preparation protocol, as introduced earlier: (i) the oscillator is initialized in a Fock state $|n_1\rangle$, while the qubit starts in an arbitrary superposition $\cos\theta|g\rangle + \sin\theta|e\rangle$; (ii) tunable access to MPJC interactions with arbitrary m is available; and (iii) projective qubit measurements can be performed at chosen times during the evolution dictated by the target state. Notably, we will later show that employing a two-step generation protocol—rather than a single-step approach—can reduce the required value of m by a factor of two, significantly easing experimental demands.

According to the first assumption, the initial joint state of the system can be written as

$$|\Psi(0)\rangle = \cos\theta|g, n_1\rangle + \sin\theta|e, n_1\rangle, \quad (5)$$

where the notation is self-evident. It is important to emphasize that neither the standard JC Hamiltonian nor its multiphoton generalization (MPJC) can generate coherence within either subsystem if the joint system initially lacks coherence [63, 78]. In the case of the spin, this is because H_{int} merely rotates the Bloch vector trivially along the z -axis [78]. As we will demonstrate, initial coherence in the qubit (parametrized by the angle θ) is essential for generating the desired superpositions in the oscillator.

We now turn to the time-evolved state vector $|\psi(t)\rangle$, governed by the interaction Hamiltonian H_{int} in Eq. (4), starting from a pure initial product state $|\psi(0)\rangle$ in Eq. (5). It is straightforward to show that the evolved state has the form

$$|\Psi(\tau)\rangle = x_1(\tau)|g, n_1\rangle + x_2(\tau)|e, n_1\rangle + x_3(\tau)|g, n_1 + m\rangle + x_4(\tau)|e, n_1 - m\rangle, \quad (6)$$

where the time-dependent coefficients are found to be

$$x_1(\tau) = \cos\theta \cos\left(\sqrt{n_1!/(n_1 - m)!}\tau\right), \quad (7a)$$

$$x_2(\tau) = \sin\theta \cos\left(\sqrt{(n_1 + m)!/n_1!}\tau\right), \quad (7b)$$

$$x_3(\tau) = -i \sin\theta \sin\left(\sqrt{(n_1 + m)!/n_1!}\tau\right), \quad (7c)$$

$$x_4(\tau) = -i \cos\theta \sin\left(\sqrt{n_1!/(n_1 - m)!}\tau\right), \quad (7d)$$

where $\tau = gt$ denotes the dimensionless scaled interaction time (see Appendix A for details).

In the following, we exploit the joint state $|\psi(\tau)\rangle$ to generate all desired superpositions of two Fock states. Our main protocol is probabilistic, relying on projective measurement of the qubit to herald the target oscillator state. We focus on this approach due to its ability to achieve higher fidelities and greater flexibility in parameter selection. For completeness, we also examine a deterministic generation protocol that avoids qubit measurement by tracing over the qubit degrees of freedom. The details of this alternative method, along with its limitations and comparative performance, are discussed in Appendix B.

IV. SUPERPOSITION OF TWO FOCK STATES

Upon projective measurement of the qubit, if it is found in the ground state $|g\rangle$, the corresponding (unnormalized) oscillator state is given by $|\psi_o(\tau)\rangle_g = x_1(\tau)|n_1\rangle + x_3(\tau)|n_1 + m\rangle$, as follows directly from Eq. (6). It is important to note that this state cannot be used to generate any of the desired binomial superposition states, as it requires m to be much greater than n_1 , which is not feasible.

On the other hand, if the qubit is in the excited state $|e\rangle$ after measurement, the resulting oscillator state is $|\psi_o(\tau)\rangle_e = \mathcal{N}\{x_2(\tau)|n_1\rangle + x_4(\tau)|n_1 - m\rangle\}$, where \mathcal{N} is the normalization constant. It is important to emphasize that, to obtain the exact superposition states, a local phase correction must be applied to eliminate the relative phase factor $-i$ preceding the state $|n_1 - m\rangle$. However, we mention in passing that a recent work on phase-engineered bosonic quantum codes [83] has shown that allowing structured sign choices in the codewords—rather than enforcing uniform phases—can improve loss tolerance. This suggests that, in certain regimes, preserving rather than correcting such phase factors could lead to enhanced error resilience.

Since the evolved state $|\psi_o(\tau)\rangle_e$ has support only on the two Fock states $|n_1\rangle$ and $|n_1 - m\rangle$, this correction can be trivially accomplished in this effective two-dimensional space as $|\psi'_o(\tau)\rangle_e = U|\psi_o(\tau)\rangle_e$, where $U = \text{diag}(1, i)$. Following this phase adjustment, the

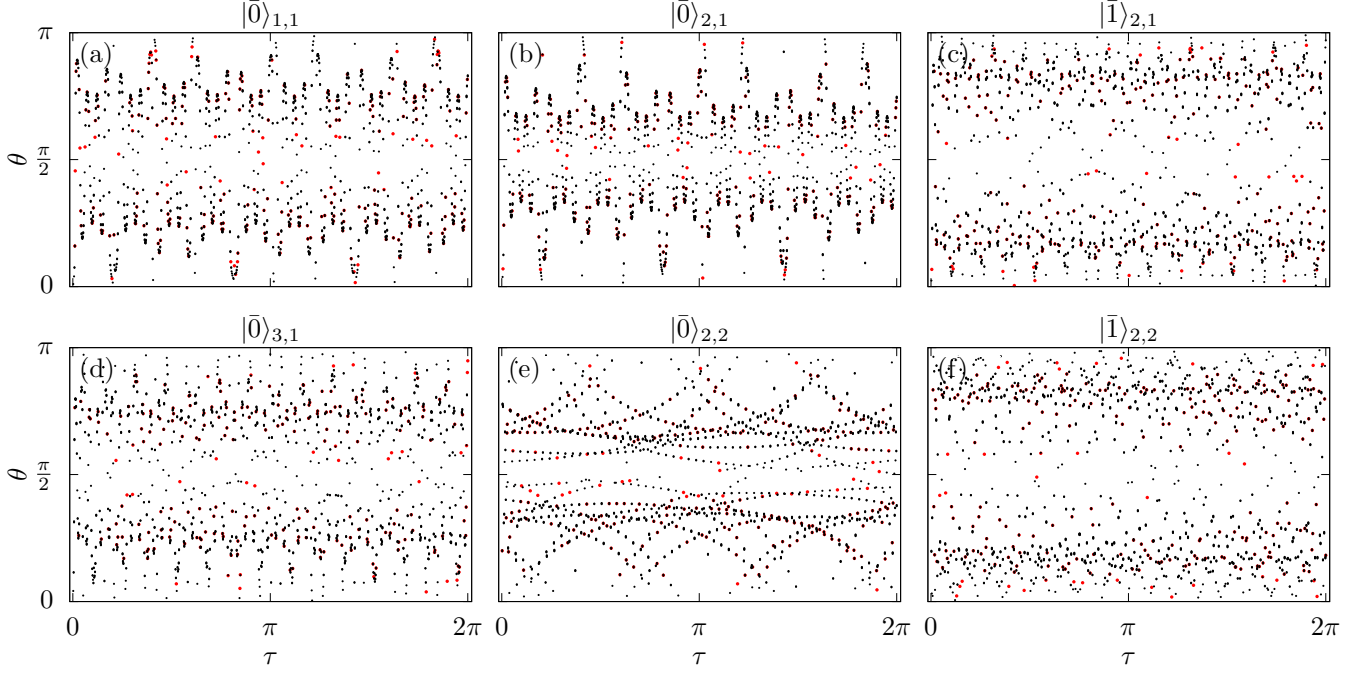


Figure 2. Combinations of $\{\tau, \theta\}$ for which the fidelity of the time-evolved oscillator state in Eq. (8) matches that of the target logical binomial states $|\bar{0}\rangle_{1,1}$, $|\bar{0}\rangle_{2,1}$, $|\bar{1}\rangle_{2,1}$, $|\bar{1}\rangle_{3,1}$, $|\bar{0}\rangle_{2,2}$, and $|\bar{1}\rangle_{2,2}$ with unit fidelity are shown in panels (a) – (f), respectively. The parameters τ and θ were sampled uniformly over $0 \leq \tau \leq 2\pi$ and $0 \leq \theta \leq \pi$, using 1001 and 501 points, respectively. All points satisfy a numerical fidelity threshold of $|F - 1| \leq 10^{-4}$, with red points indicating those that additionally meet the stricter criterion $|F - 1| \leq 10^{-6}$.

oscillator is left in the target superposition state

$$|\psi'_o(\tau)\rangle_e = \mathcal{N} \left\{ \sin \theta \cos(a_{n_1, m} \tau) |n_1\rangle + \cos \theta \sin(b_{n_1, m} \tau) |n_1 - m\rangle \right\}, \quad (8)$$

where $\mathcal{N} = [\cos^2 \theta \sin^2(a_{n_1, m} \tau) + \sin^2 \theta \cos^2(b_{n_1, m} \tau)]^{-\frac{1}{2}}$, $a_{n_1, m} = \sqrt{(n_1 + m)!/n_1!}$, and $b_{n_1, m} = \sqrt{n_1!/(n_1 - m)!}$. It can be shown that, with judicious choices of n_1 and m , and by appropriately tuning the parameters θ and τ , arbitrary superpositions of any two target Fock states can be systematically synthesized. For completeness, we work out some specific examples in the following.

The states corresponding to $n_1 = m = 4$, and $n_1 = 6$ and $m = 4$ are

$$|\psi'_{o1}(\tau)\rangle = \mathcal{N}_1 \{ \cos \theta \sin(a_{4,4} \tau) |0\rangle + \sin \theta \cos(b_{4,4} \tau) |4\rangle \}, \quad (9)$$

$$|\psi'_{o2}(\tau)\rangle = \mathcal{N}_2 \{ \cos \theta \sin(a_{6,4} \tau) |2\rangle + \sin \theta \cos(b_{6,4} \tau) |6\rangle \}, \quad (10)$$

where $\mathcal{N}_1 = [\cos^2 \theta \sin^2(a_{4,4} \tau) + \sin^2 \theta \cos^2(b_{4,4} \tau)]^{-\frac{1}{2}}$, $\mathcal{N}_2 = [\cos^2 \theta \sin^2(a_{6,4} \tau) + \sin^2 \theta \cos^2(b_{6,4} \tau)]^{-\frac{1}{2}}$, with $a_{4,4} = \sqrt{4!}$, $b_{4,4} = \sqrt{8!/4!}$, $a_{6,4} = \sqrt{6!/2!}$, and $b_{6,4} = \sqrt{10!/6!}$. The fidelities of the states $|\psi'_{o1}(\tau)\rangle$ and $|\psi'_{o2}(\tau)\rangle$ with the arbitrary target states of the form $|\phi\rangle_1 =$

$c_1 |0\rangle + \bar{c}_1 |4\rangle$, and $|\phi\rangle_2 = c_2 |2\rangle + \bar{c}_2 |6\rangle$, are given by

$$F_1 = \mathcal{N}_1^2 |c_1 \cos \theta \sin(a_{4,4} \tau) + \bar{c}_1 \sin \theta \cos(b_{4,4} \tau)|^2, \quad (11)$$

$$F_2 = \mathcal{N}_2^2 |c_2 \cos \theta \sin(a_{6,4} \tau) + \bar{c}_2 \sin \theta \cos(b_{6,4} \tau)|^2, \quad (12)$$

respectively. Here, $\bar{c}_i = \sqrt{1 - c_i^2}$ with $i = 1, 2$. Now, the fidelities F_1 and F_2 can reach unity for any choice of the coefficients c_1 and c_2 . As shown in Fig. 2(a-d), we numerically identify all combinations of θ and τ for which the logical states $|\bar{0}\rangle_{1,1}$, $|\bar{0}\rangle_{2,1}$, $|\bar{1}\rangle_{2,1}$, and $|\bar{1}\rangle_{3,1}$ are realized with unit fidelity, up to a numerical tolerance of 10^{-4} . The highlighted red points in all panels satisfy a much stricter tolerance of 10^{-6} . It is evident from all panels that multiple parameter combinations enable the realization of the target states.

On the other hand, the states corresponding to $n_1 = m = 6$, and $n_1 = 9$ and $m = 6$ are

$$|\psi'_{o3}(\tau)\rangle = \mathcal{N}_3 \{ \cos \theta \sin(a_{6,6} \tau) |0\rangle + \sin \theta \cos(b_{6,6} \tau) |6\rangle \}, \quad (13)$$

$$|\psi'_{o4}(\tau)\rangle = \mathcal{N}_4 \{ \cos \theta \sin(b_{9,6} \tau) |3\rangle + \sin \theta \cos(b_{9,6} \tau) |9\rangle \}, \quad (14)$$

where $\mathcal{N}_3 = [\cos^2 \theta \sin^2(a_{6,6} \tau) + \sin^2 \theta \cos^2(b_{6,6} \tau)]^{-\frac{1}{2}}$, and $\mathcal{N}_4 = [\cos^2 \theta \sin^2(a_{9,6} \tau) + \sin^2 \theta \cos^2(b_{9,6} \tau)]^{-\frac{1}{2}}$, with $a_{6,4} = \sqrt{6!}$, $b_{6,6} = \sqrt{12!/6!}$, $a_{9,6} = \sqrt{9!/3!}$, and $b_{9,6} = \sqrt{15!/9!}$. The fidelities of the states $|\psi'_{o3}(\tau)\rangle$ and $|\psi'_{o4}(\tau)\rangle$ with the arbitrary target states of the form

$|\phi\rangle_3 = c_3 |0\rangle + \bar{c}_3 |6\rangle$, and $|\phi\rangle_4 = c_4 |3\rangle + \bar{c}_4 |9\rangle$, are given by

$$F_3 = \mathcal{N}_3^2 |c_3 \cos \theta \sin(a_{6,6}\tau) + \bar{c}_3 \sin \theta \cos(b_{6,6}\tau)|^2, \quad (15)$$

$$F_4 = \mathcal{N}_4^2 |c_4 \cos \theta \sin(a_{9,6}\tau) + \bar{c}_4 \sin \theta \cos(b_{9,6}\tau)|^2, \quad (16)$$

respectively. Here $\bar{c}_i = \sqrt{1 - c_i^2}$ with $i = 3, 4$. All combinations of θ and τ for which the logical states $|\bar{0}\rangle_{2,2}$ and $|\bar{1}\rangle_{2,2}$ are realized with unit fidelity are depicted in Fig. 2(e,f). Similar to the previous cases, we again find multiple parameter combinations that achieve the target binomial code states with unit fidelity.

It is straightforward to verify that, by following a similar procedure, arbitrary superpositions of two Fock states can be realized. In the following section, we extend this approach to generate superpositions of three Fock states.

V. SUPERPOSITION OF THREE FOCK STATES

In the preceding section, we demonstrated that, by employing the MPJC Hamiltonian and appropriately selecting the initial configurations, arbitrary superpositions of two Fock states can be engineered. In what follows, we show how this method can be extended to synthesize superpositions of three Fock states with high fidelity, by using an initial oscillator state that is itself an arbitrary superposition of two Fock states, along with an initial arbitrary superposition of the qubit basis states. That is, we assume the initial state for the bipartite system to be

$$|\Psi(0)\rangle = (\cos \theta |g\rangle + \sin \theta |e\rangle) \otimes (\cos \phi |n_1\rangle + \sin \phi |n_2\rangle). \quad (17)$$

It is worth noting that, although such an initial state formally departs from our first assumption, we showed in the previous section that arbitrary two-Fock superpositions can still be generated using the MPJC Hamiltonian. Building on this, three-Fock-state superpositions can be realized in a two-step protocol: first prepare a two-Fock resource state, then extend it to the desired three-Fock superposition. It can be straightforwardly shown that the time-evolved state vector for such an initial state can be expressed as

$$|\Psi(\tau)\rangle = x_1(\tau) |g, n_1\rangle + x_2(\tau) |e, n_1\rangle + x_3(\tau) |g, n_1 + m\rangle + x_4(\tau) |e, n_1 - m\rangle + y_1(\tau) |g, n_2\rangle + y_2(\tau) |e, n_2\rangle + y_3(\tau) |g, n_2 + m\rangle + y_4(\tau) |e, n_2 - m\rangle. \quad (18)$$

where the time-dependent coefficients can be found in Appendix A (see Eq. (A3)). Note that Eqs. (6) and (7) are special cases of Eqs. (18) and (A3), respectively, which are recovered by setting $\phi = 0$.

Now, suppose a projective measurement on the qubit is carried out and it is found in the ground state $|g\rangle$. In that case, it can be readily shown that, similar to

the two-state case, it is not possible to realize arbitrary superpositions of three Fock states.

On the other hand, after the measurement, if the qubit is found in the excited state $|e\rangle$, we obtain an oscillator state $|\psi_o(\tau)\rangle_e = \mathcal{N}\{x_2(\tau) |n_1\rangle + x_4(\tau) |n_1 - m\rangle + y_2(\tau) |n_2\rangle + y_4(\tau) |n_2 - m\rangle\}$. Once again, to obtain the correct superposition states, it is necessary to perform a local phase correction to eliminate the negative i factors preceding the states $|n_1 - m\rangle$ and $|n_2 - m\rangle$. This can be achieved by applying a unitary transformation $U = \text{diag}(1, i, 1, i)$ such that $|\psi'_o(\tau)\rangle_e = U |\psi_o(\tau)\rangle_e$. After this local phase correction, we obtain

$$|\psi'_o(t)\rangle_e = \mathcal{N}\{x_2(\tau) |n_1\rangle + x'_4(\tau) |n_1 - m\rangle + y_2(\tau) |n_2\rangle + y'_4(\tau) |n_2 - m\rangle\}, \quad (19)$$

where $x'_4(\tau) = ix_4(\tau)$, $y'_4(\tau) = iy_4(\tau)$, and the normalization $\mathcal{N} = [x_2^2 + x_4'^2 + y_2^2 + y_4'^2]^{-\frac{1}{2}}$.

It is evident that, by appropriately choosing n_1 , n_2 , and m , arbitrary superpositions of three Fock states can be realized. In the following, we illustrate this with a few explicit examples. These are the binomial code states $|\bar{0}\rangle_{3,1}$, $|\bar{0}\rangle_{4,1}$, $|\bar{1}\rangle_{4,1}$, $|\bar{1}\rangle_{5,1}$, as defined earlier.

Note that the states $|\bar{0}\rangle_{3,1}$ and $|\bar{0}\rangle_{4,1}$, which are superpositions of $|0\rangle$, $|4\rangle$, and $|8\rangle$, can be generated by setting $n_1 = m = 4$ and $n_2 = 8$. Similarly, the states $|\bar{1}\rangle_{4,1}$ and $|\bar{1}\rangle_{5,1}$, which are superpositions of $|2\rangle$, $|6\rangle$, and $|10\rangle$, can be realized by choosing $n_1 = 6$, $m = 4$, and $n_2 = 10$. Substituting these parameter values into Eq. (19), we obtain the corresponding states in the following compact forms

$$|\psi'_{o1}(\tau)\rangle = \mathcal{N}_1 \{C_0 |0\rangle + C_4 |4\rangle + C_8 |8\rangle\}, \quad (20)$$

$$|\psi'_{o2}(\tau)\rangle = \mathcal{N}_2 \{C_2 |2\rangle + C_6 |6\rangle + C_{10} |10\rangle\}, \quad (21)$$

where \mathcal{N}_1 and \mathcal{N}_2 are the appropriate normalization constants. Further, $C_0 = \cos \theta \cos \phi \sin(\tau_0)$, $C_2 = \cos \theta \cos \phi \sin(\tau_2)$, $C_4 = \sin \theta \cos \phi \cos(\tau_4) + \cos \theta \sin \phi \sin(\tau_4)$, $C_6 = \sin \theta \cos \phi \cos(\tau_6) + \cos \theta \sin \phi \sin(\tau_6)$, $C_8 = \sin \theta \sin \phi \cos(\tau_8)$, and $C_{10} = \sin \theta \sin \phi \cos(\tau_{10})$, where $\tau_0 = \sqrt{4!}\tau$, $\tau_2 = \sqrt{6!}/2!\tau$, $\tau_4 = \sqrt{8!}/4!\tau$, $\tau_6 = \sqrt{10!}/6!\tau$, $\tau_8 = \sqrt{12!}/8!\tau$, and $\tau_{10} = \sqrt{14!}/10!\tau$.

Now, the expressions for the fidelities corresponding to the four different binomial code states $|\bar{0}\rangle_{3,1}$, $|\bar{0}\rangle_{4,1}$, $|\bar{1}\rangle_{4,1}$, and $|\bar{1}\rangle_{5,1}$ can be straightforwardly obtained. They are given by

$$F_1 = \frac{\mathcal{N}_1^2}{8} |C_0 + \sqrt{6} C_4 + C_8|^2 \quad (22)$$

$$F_2 = \frac{\mathcal{N}_1^2}{16} |C_0 + \sqrt{10} C_4 + \sqrt{5} C_8|^2, \quad (23)$$

$$F_3 = \frac{\mathcal{N}_2^2}{16} |\sqrt{5} C_2 + \sqrt{10} C_6 + C_{10}|^2, \quad (24)$$

$$F_4 = \frac{\mathcal{N}_2^2}{32} |\sqrt{6} C_2 + \sqrt{20} C_6 + \sqrt{6} C_{10}|^2. \quad (25)$$

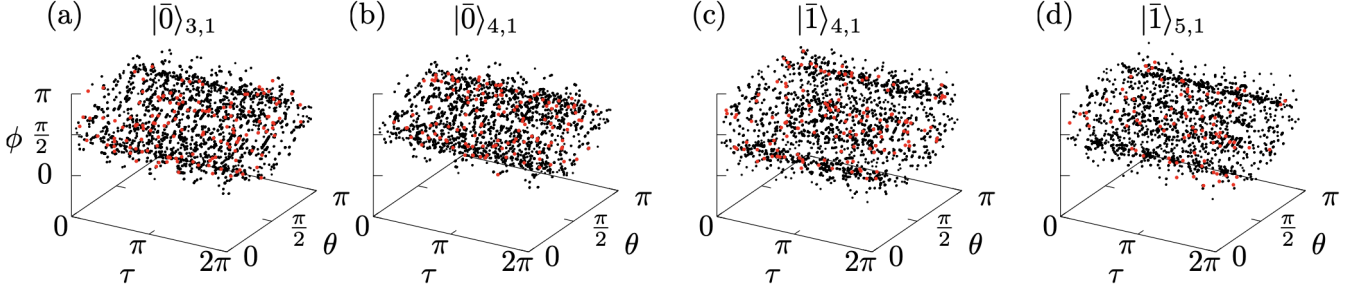


Figure 3. Combinations of $\{\tau, \theta, \phi\}$ for which the fidelities of the time-evolved oscillator states in Eq. (19) match the target logical states $|\bar{0}\rangle_{3,1}$, $|\bar{0}\rangle_{4,1}$, $|\bar{1}\rangle_{4,1}$, and $|\bar{1}\rangle_{5,1}$ with unit fidelity are shown in panels (a) – (d), respectively. A total of 1001 (501) values of τ (θ and ϕ) were sampled numerically over the ranges $0 \leq \tau \leq 2\pi$ ($0 \leq \theta, \phi \leq \pi$). Similar to Fig. 2, all points satisfy a numerical fidelity threshold of $|F - 1| \leq 10^{-4}$, with red points indicating those that additionally meet the stricter criterion $|F - 1| \leq 10^{-6}$.

The task thus reduces to optimizing the parameters θ , ϕ , and τ to achieve unit fidelity. We have carried out this optimization numerically by scanning $\theta \in [0, \pi]$, $\phi \in [0, \pi]$, and $\tau \in [0, 2\pi]$ with a resolution of 501 points for θ and ϕ , and 1001 points for τ . As in the previous case, numerous parameter combinations yield fidelities equal to unity. Specifically, we identify 14809 valid parameter sets for F_1 , 13311 for F_2 , 13601 for F_3 , and 10752 for F_4 , each achieving unit fidelity within a numerical precision of 10^{-4} . These optimal combinations are visualized as scatter plots in Fig. 3, highlighting the substantial flexibility in selecting parameters for synthesizing the target code states. As anticipated, increasing the numerical precision reduces the number of viable solutions. Under a stricter tolerance of 10^{-6} , the number of matches drops to 151, 131, 139, and 89, respectively, marked as red points in the plots.

Before proceeding, we note that this procedure can be systematically extended to generate larger superpositions involving four or more Fock states. An explicit example for a four-component state is provided in the Appendix A. Importantly, as the number of target Fock components increases, the number of required MPJC interaction steps grows accordingly, leading to a corresponding increase in the computational overhead for numerical optimization.

VI. REDUCING ORDER OF MULTIPHOTON INTERACTIONS

Thus far, in engineering binomial code states, we have observed that increasing the number of correctable losses (S) necessitates a corresponding increase in the value of m . As a result, generating code states with large S rapidly becomes practically infeasible. In this section, we address this limitation and demonstrate that the required m can, in fact, be reduced by a factor of two when the code states are superpositions of two Fock states. This comes at the cost of increasing the number of times the MPJC needs to be implemented. Recall that

with the one-step MPJC process, it is possible to create states which are superpositions of $|n_1\rangle$ and $|n_1 - m\rangle$ (as shown in Eq. (8)). Instead, if we use the state $|\psi_o(\tau)\rangle_e$ in Eq. (19) and set $n_2 = n_1 - m$, the unnormalized oscillator state takes the form

$$\begin{aligned} |\psi'_o(t)\rangle_e = & \cos \theta \sin \phi \sin \left(\sqrt{\frac{(n_1 - m)!}{(n_1 - 2m)!}} \tau \right) |n_1 - 2m\rangle \\ & + \left\{ \cos \theta \cos \phi \sin \left(\sqrt{\frac{n_1!}{(n_1 - m)!}} \tau \right) \right. \\ & \quad \left. + \sin \theta \sin \phi \cos \left(\sqrt{\frac{n_1!}{(n_1 - m)!}} \tau \right) \right\} |n_1 - m\rangle \\ & + \sin \theta \cos \phi \cos \left(\sqrt{\frac{(n_1 + m)!}{n_1!}} \tau \right) |n_1\rangle. \end{aligned} \quad (26)$$

It is evident that whenever the coefficient of $|n_1 - m\rangle$ vanishes, the oscillator state reduces to a superposition of $|n_1\rangle$ and $|n_1 - 2m\rangle$. In general, this state may not exactly coincide with the target binomial code state. In other words, the superposition coefficients may not match exactly with the target state. In such cases, an additional unitary operation must be applied to transform the oscillator state into the desired target state. Let us work out a couple of example cases.

For example, we previously demonstrated that the states $|\bar{0}\rangle_{1,1} = (|0\rangle + |4\rangle)/\sqrt{2}$ and $|\bar{0}\rangle_{2,2} = (|0\rangle + \sqrt{3}|6\rangle)/2$ can be generated using $n_1 = 4$, $m = 4$, and $n_1 = 6$, $m = 6$, respectively. With the two-step protocol, however, these same states can be achieved with reduced multiphoton orders $m = 2$ and $m = 3$. Substituting the corresponding values of n_1 and m into Eq. (26), we obtain oscillator states that are superpositions of $|0\rangle$, $|2\rangle$, and $|4\rangle$ or $|0\rangle$, $|3\rangle$, and $|6\rangle$. The coefficients of the intermediate states $|2\rangle$ and $|3\rangle$, respectively, are given (up to normalization) by

$$C_k(\tau, \theta, \phi) = \cos \theta \cos \phi \sin \tau_k + \sin \theta \sin \phi \cos \tau_k, \quad (27)$$

with $k = 2, 3$, where $\tau_2 = \sqrt{12}, \tau$ and $\tau_3 = \sqrt{120}, \tau$.

The optimal parameter sets for which the functions C_2 and C_3 vanish (within a numerical precision of 10^{-4}) are

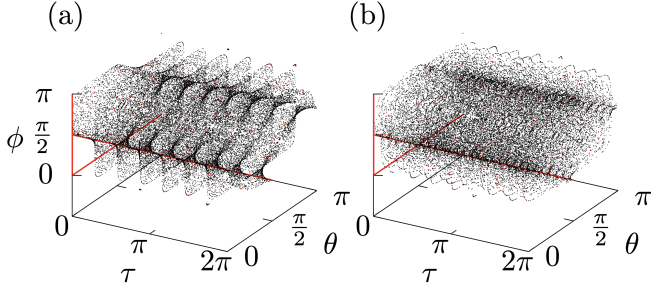


Figure 4. Combinations of $\{\tau, \theta, \phi\}$ for which the functions C_2 and C_3 defined in Eq. (27) vanish. Numerical sampling was performed over 1001 values of τ in the range $[0, 2\pi]$ and 501 values each for θ and ϕ in $[0, \pi]$. All displayed points satisfy a numerical tolerance of $\leq 10^{-4}$, while red points highlight those meeting a stricter threshold of $\leq 10^{-6}$.

shown as scatter plots in Fig. 4. A large number of valid combinations are observed, highlighting the flexibility of the protocol. Selecting any such combination yields oscillator states of the form $\alpha_2 |0\rangle + \beta_2 |4\rangle$ and $\alpha_3 |0\rangle + \beta_3 |6\rangle$, respectively. The final step involves applying suitable unitary operations to transform these intermediate states into the desired target states with high fidelity.

Before proceeding, we emphasize that the scheme described in this section applies exclusively to code states comprising superpositions of two Fock states. Moreover, the reduction in the required m value by a factor of two is a one-time improvement; further reductions by factors of 4, 8, and so on are not supported within this approach.

VII. ENVIRONMENTAL EFFECTS

Until now, our analysis has focused exclusively on ideal unitary evolution of the bipartite quantum system, neglecting the critical effects of system–environment interactions. In the following, we extend the study to incorporate these effects through numerical simulations, examining how environmental couplings affect the fidelity of the code states. We adopt the standard Lindblad formalism, which relies on the Markovian approximation and other common assumptions such as the Born and secular approximations. Within this framework, the evolution of the reduced density matrix of the bipartite system, $\rho_S(t)$, is governed by the Lindblad master equation

$$\frac{d\rho_S}{dt} = -i[H, \rho_S] + \sum_k \left(L_k \rho_S L_k^\dagger - \frac{1}{2} [\rho_S, L_k^\dagger L_k] \right). \quad (28)$$

Here, $L_k = \sqrt{\lambda_k} A_k$ are the collapse (Lindblad) operators, where the environment couples to the system through operators A_k with corresponding rates λ_k . To simplify the numerical analysis, we assume that both the oscillator and the two-level system interact with a common thermal environment at a temperature characterized by the mean thermal occupation \bar{n}_{th} .

For the bosonic mode, the relevant Lindblad operators are $\sqrt{\lambda_{os_r}(1 + \bar{n}_{\text{th}})} a$, $\sqrt{\lambda_{os_d} \bar{n}_{\text{th}}} a^\dagger$, and $\sqrt{\lambda_{os_d}} a^\dagger a$ which lead to emission/relaxation, absorption, and dephasing effects, respectively. Similarly, for the two-level system, the corresponding Lindblad operators are $\sqrt{\lambda_{qb_r}(1 + \bar{n}_{\text{th}})} \sigma_-$, $\sqrt{\lambda_{qb_a} \bar{n}_{\text{th}}} \sigma_+$, and $\sqrt{\lambda_{qb_d}} \sigma_z$. While both relaxation and absorption rates depend on the bath temperature \bar{n}_{th} , the dephasing rates are temperature-independent. For simplicity, we assume $\lambda_{os_r} = \lambda_{os_d}$, and $\lambda_{qb_r} = \lambda_{qb_a}$.

To illustrate the impact of system–environment interactions on state preparation, we consider a representative example: the logical codeword $|\bar{0}\rangle_{1,1}$. While our analysis focuses on this specific case, we have verified that qualitatively similar behavior is observed for other logical states constructed as superpositions of two Fock states. To streamline the analysis and mitigate the effects of decoherence, we fix the parameter θ to the value at which the fidelity first reaches unity (within a numerical threshold of 10^{-6}) in the absence of dissipation. This choice minimizes additional infidelity arising from the interaction with the environment. For the state $|\bar{0}\rangle_{1,1}$, we find numerically that this occurs at $t = 0.037699$ with the corresponding $\theta = 1.432566$.

We first consider the case of zero temperature ($\bar{n}_{\text{th}} = 0$), where decoherence arises exclusively from vacuum fluctuations—i.e., energy relaxation and dephasing in the absence of thermal excitations [see Fig. 5(a)]. The relevant collapse operators governing the open-system dynamics are $\sqrt{\lambda_{os_r}} a$ and $\sqrt{\lambda_{os_d}} a^\dagger a$ for the oscillator, and $\sqrt{\lambda_{qb_r}} \sigma_-$ and $\sqrt{\lambda_{qb_d}} \sigma_z$ for the qubit. We analyze three distinct scenarios: (i) the oscillator is coupled to the environment (red curves), (ii) the qubit is coupled (blue curves), and (iii) both subsystems are coupled simultaneously (black curves). In all cases, dashed and dotted lines correspond to pure dissipation and pure dephasing, respectively, while solid lines represent the combined influence of both. Notably, dephasing alone leads to a much lesser fidelity loss than energy relaxation for equivalent rates. Furthermore, the fidelity is more severely degraded when the qubit is coupled to the bath, as compared to the case in which the oscillator only interacts with the environment.

The effect of finite thermal excitations ($\bar{n}_{\text{th}} > 0$) is illustrated in Figs. 5(b) and 5(c), where all relevant Lindblad operators actively contribute to the system’s open dynamics. As expected, the pure dephasing curves remain identical across panels, reflecting their insensitivity to thermal excitations. In contrast, increasing the thermal occupation number \bar{n}_{th} leads to a progressive reduction in fidelity for all remaining cases, underscoring the detrimental role of thermal noise on the robustness of the encoded state.

For code states involving superpositions of a larger number of Fock states, the detrimental impact of losses is expected to be more pronounced. This is due to the fact that generating such states requires multiple sequential implementations of the MPJC interaction, with each

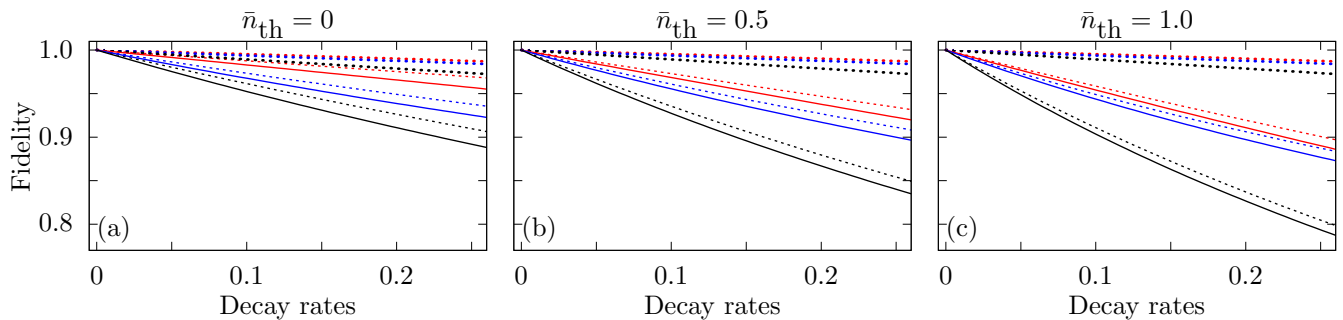


Figure 5. Fidelity degradation of the logical state $|\bar{0}\rangle_{1,1}$ as a function of the decay rates, under the influence of system–environment interactions. Panels (a)–(c) correspond to increasing thermal bath occupations \bar{n}_{th} , as indicated above each panel. The values of θ and τ are fixed to those for which the fidelity first reaches unity (within a numerical precision of 10^{-6}) in the ideal, dissipation-free case. Three dissipation scenarios are considered: (i) oscillator-only coupling (red), (ii) qubit-only coupling (blue), and (iii) joint coupling of both subsystems to a common bath (black). In each case, dashed and dotted lines denote the effects of pure dissipation and pure dephasing, respectively, while solid lines represent the combined influence of both channels.

stage introducing additional exposure to decoherence. As a result, losses compound over the course of the protocol, leading to a cumulative degradation in fidelity. However, by carefully selecting an optimal interaction time at each step—preferably at the earliest instance when high fidelity is achieved—the effects of losses can be mitigated to a certain extent.

VIII. CONCLUDING REMARKS

Rotation-symmetric bosonic codes (RBSCs) encode quantum information in states invariant under discrete phase-space rotations, leveraging rotation symmetries to enhance error resilience and fault tolerance [14, 69, 84]. Various families of RBSCs have been proposed, including (squeezed) cat codes [30–33, 85, 86], Pegg–Barnett codes [25], GKP-like codes [10, 23], and binomial codes [10, 48]. In this work, we focus on the binomial code family, which consists of finite superpositions of Fock states with coefficients drawn from a binomial distribution.

We have presented a general and high-fidelity scheme for synthesizing *arbitrary* binomial codewords by harnessing nonlinear multiphoton interactions between a bosonic mode (oscillator) and a two-level system (qubit). Our approach is based on the coherent dynamics of the multiphoton Jaynes–Cummings (MPJC) Hamiltonian and assumes experimentally reasonable capabilities: initialization of the oscillator and qubit, access to multiphoton interactions, and qubit measurements during the evolution. While iterative methods based on standard cavity QED interactions have proven effective for generating cat codes starting from easily prepared coherent states, a similar strategy is less practical for binomial codes. As discussed in Appendix C, the primitive states required for binomial codewords are themselves complex superpositions of Fock states and do not offer a clear experimental advantage over direct codeword generation.

A key insight from our analysis is the essential role of a coherent initial qubit state in generating superpositions of target Fock states. This requirement stems from the inability of the MPJC Hamiltonian to induce coherence in either subsystem if the joint initial state lacks it—a constraint highlighted in recent studies [63, 78]. More broadly, the challenge of harnessing noisy or incoherent resources for generating entanglement and coherence remains an active area of investigation [87–89]. This raises an important question: can the inclusion of an additional dispersive spin-boson interaction compensate for the coherence shortfall of MPJC dynamics and enable high-fidelity synthesis of bosonic code states using noisy initial resources? The authors aim to address this issue in the future.

Another important feature in our scheme is the ability to reduce the required multiphoton transition order by a factor of two without sacrificing fidelity, thus significantly enhancing the experimental feasibility of the protocol. This one-time improvement is achieved by judiciously selecting the initial oscillator state and exploiting coherent interference effects.

In developing our protocol, we explored two complementary approaches to generating binomial codewords. The probabilistic protocol, which relies on projective measurement of the qubit after joint evolution, offers higher fidelities and greater flexibility in scanning the parameter space, making it better suited for precise codeword synthesis. However, a key drawback of this approach is its inherent probabilistic nature—only a subset of measurement outcomes yield the desired oscillator state, resulting in a trade-off between fidelity and generation efficiency. In contrast, the deterministic protocol, which involves tracing out the qubit degrees of freedom without any measurement, is operationally simpler and potentially more suitable in scenarios where projective measurements are inefficient, technically challenging, or resource-intensive. Due to the constrained parameter space accessible in the deterministic setting, this proto-

col typically achieves slightly lower fidelities. A detailed comparison, along with results for the deterministic protocol, is provided in Appendix B.

Our results contribute to the broader effort of realizing fault-tolerant bosonic quantum computing, not only by identifying an efficient method for preparing logical code-words, but also by highlighting the utility of nonlinear light-matter interactions in continuous-variable quantum systems. The methods outlined here are versatile and can be extended to prepare larger classes of bosonic code-words, potentially including cat codes and other non-Gaussian encodings.

In summary, this work provides a scalable and practical pathway toward high-fidelity generation of binomial code states, addressing a critical bottleneck in the realization of bosonic quantum error correction.

ACKNOWLEDGMENTS

We thank P. A. Ameen Yasir and S. Siddardha Cheluri for valuable discussions. We acknowledge funding from the BMBF in Germany (QR.X, PhotonQ, QuKuK, QuaPhySI), from the Deutsche Forschungsgemeinschaft (DFG, German Research Foundation) – Project-ID 429529648 – TRR 306 QuCoLiMa (“Quantum Cooperativity of Light and Matter”), and also from the EU project CLUSTEC (grant agreement no. 101080173).

Appendix A: Details on the state vector

In this section, we present additional details on the oscillator state vectors obtained through our protocol for generating binomial codewords involving superpositions of two and three Fock states. Furthermore, we extend our analysis to include a representative example of a superposition of four Fock states, illustrating the scalability of the protocol to more complex codewords.

1. Superposition of two Fock states

Applying the time-independent Schrödinger equation, $i\frac{d}{dt}|\Psi(t)\rangle = H_{\text{int}}|\Psi(t)\rangle$, with H_{int} and $|\Psi(t)\rangle$ as defined in Eqs. (4) and (6), respectively, we get four time-dependent coefficients that obey the following coupled differential equations

$$i\dot{x}_1(\tau) = \sqrt{n_1!/(n_1 - m)!} x_4(\tau), \quad (\text{A1a})$$

$$i\dot{x}_2(\tau) = \sqrt{(n_1 + m)!/n_1!} x_3(\tau), \quad (\text{A1b})$$

$$i\dot{x}_3(\tau) = \sqrt{(n_1 + m)!/n_1!} x_2(\tau), \quad (\text{A1c})$$

$$i\dot{x}_4(\tau) = \sqrt{n_1!/(n_1 - m)!} x_1(\tau), \quad (\text{A1d})$$

where $\tau = gt$. The initial condition in Eq.(5) implies $x_1(0) = \cos\theta$, $x_2(0) = \sin\theta$, and $x_3(0) = x_4(0) = 0$.

Solving the coupled differential equations with these initial values yields explicit expressions for all four time-dependent coefficients. The resulting solutions are provided in Eq. (7) of the main text.

2. Superposition of three Fock states

Following the same procedure as outlined earlier, and using the state $|\Psi(t)\rangle$ defined in Eq.(18), we obtain a set of eight coupled differential equations describing the system’s time evolution. The first four equations are identical to the ones presented in Eq.(A1), while the remaining four are given by

$$i\dot{y}_1(\tau) = \sqrt{n_2!/(n_2 - m)!} y_4(\tau), \quad (\text{A2a})$$

$$i\dot{y}_2(\tau) = \sqrt{(n_2 + m)!/n_2!} y_3(\tau), \quad (\text{A2b})$$

$$i\dot{y}_3(\tau) = \sqrt{(n_2 + m)!/n_2!} y_2(\tau), \quad (\text{A2c})$$

$$i\dot{y}_4(\tau) = \sqrt{n_2!/(n_2 - m)!} y_1(\tau). \quad (\text{A2d})$$

The initial conditions are given by $x_1(0) = \cos\theta \cos\phi$, $x_2(0) = \sin\theta \cos\phi$, $y_1(0) = \cos\theta \sin\phi$, and $y_2(0) = \sin\theta \sin\phi$, with all other coefficients vanishing initially: $x_3(0) = x_4(0) = y_3(0) = y_4(0) = 0$. Solving the resulting set of coupled differential equations yields

$$x_1(\tau) = \cos\theta \cos\phi \cos\left(\sqrt{n_1!/(n_1 - m)!}\tau\right), \quad (\text{A3a})$$

$$x_2(\tau) = \sin\theta \cos\phi \cos\left(\sqrt{(n_1 + m)!/n_1!}\tau\right), \quad (\text{A3b})$$

$$x_3(\tau) = -i \sin\theta \cos\phi \sin\left(\sqrt{(n_1 + m)!/n_1!}\tau\right), \quad (\text{A3c})$$

$$x_4(\tau) = -i \cos\theta \cos\phi \sin\left(\sqrt{n_1!/(n_1 - m)!}\tau\right), \quad (\text{A3d})$$

$$y_1(\tau) = \cos\theta \sin\phi \cos\left(\sqrt{n_2!/(n_2 - m)!}\tau\right), \quad (\text{A3e})$$

$$y_2(\tau) = \sin\theta \sin\phi \cos\left(\sqrt{(n_2 + m)!/n_2!}\tau\right), \quad (\text{A3f})$$

$$y_3(\tau) = -i \sin\theta \sin\phi \sin\left(\sqrt{(n_2 + m)!/n_2!}\tau\right), \quad (\text{A3g})$$

$$y_4(\tau) = -i \cos\theta \sin\phi \sin\left(\sqrt{n_2!/(n_2 - m)!}\tau\right). \quad (\text{A3h})$$

3. Superposition of four Fock states

In the main text, we demonstrated that a superposition of three Fock states can be realized through appropriate choices of system parameters. Building on that result, we now show that it is also possible to generate superpositions involving four Fock states by extending the same procedure. We begin with the following initial state for the full system

$$|\Psi(0)\rangle = (\cos\theta |g\rangle + \sin\theta |e\rangle) \otimes (\sin\phi_1 \cos\phi_2 |n_1\rangle + \sin\phi_1 \sin\phi_2 |n_2\rangle + \cos\phi_1 |n_3\rangle). \quad (\text{A4})$$

It is straightforward to verify that the time-evolved state vector takes the form

$$\begin{aligned} |\Psi(\tau)\rangle = & x_1 |g, n_1\rangle + x_2 |e, n_1\rangle + x_3 |g, n_1 + m\rangle \\ & + x_4 |e, n_1 - m\rangle + y_1 |g, n_2\rangle + y_2 |e, n_2\rangle \\ & + y_3 |g, n_2 + m\rangle + y_4 |e, n_2 - m\rangle + z_1 |g, n_3\rangle \\ & + z_2 |e, n_3\rangle + z_3 |g, n_3 + m\rangle + z_4 |e, n_3 - m\rangle, \end{aligned} \quad (\text{A5})$$

where, for brevity, we have omitted the explicit time dependence of the coefficients on the right-hand side.

Proceeding as before, we derive the set of twelve coupled differential equations governing the system dynamics. The initial conditions are given by $x_1(0) = \cos \theta \sin \phi_1 \cos \phi_2$, $x_2(0) = \sin \theta \sin \phi_1 \cos \phi_2$, $y_1(0) = \cos \theta \sin \phi_1 \sin \phi_2$, $y_2(0) = \sin \theta \sin \phi_1 \sin \phi_2$, $z_1(0) = \cos \theta \cos \phi_1$, $z_2(0) = \sin \theta \cos \phi_1$, with all remaining coefficients initialized to zero: $x_3(0) = x_4(0) = y_3(0) = y_4(0) = z_3(0) = z_4(0) = 0$.

Solving the resulting system of differential equations provides the complete time evolution of the state coefficients. The x coefficients are given by

$$x_1(\tau) = \cos \theta \sin \phi_1 \cos \phi_2 \cos \left(\sqrt{n_1!/(n_1 - m)!} \tau \right), \quad (\text{A6a})$$

$$x_2(\tau) = \sin \theta \sin \phi_1 \cos \phi_2 \cos \left(\sqrt{(n_1 + m)!/n_1!} \tau \right), \quad (\text{A6b})$$

$$x_3(\tau) = -i \sin \theta \sin \phi_1 \cos \phi_2 \sin \left(\sqrt{(n_1 + m)!/n_1!} \tau \right), \quad (\text{A6c})$$

$$x_4(\tau) = -i \cos \theta \sin \phi_1 \cos \phi_2 \sin \left(\sqrt{n_1!/(n_1 - m)!} \tau \right). \quad (\text{A6d})$$

On the other hand, the y coefficients are given by

$$y_1(\tau) = \cos \theta \sin \phi_1 \sin \phi_2 \cos \left(\sqrt{n_2!/(n_2 - m)!} \tau \right), \quad (\text{A7a})$$

$$y_2(\tau) = \sin \theta \sin \phi_1 \sin \phi_2 \cos \left(\sqrt{(n_2 + m)!/n_2!} \tau \right), \quad (\text{A7b})$$

$$y_3(\tau) = -i \sin \theta \sin \phi_1 \sin \phi_2 \sin \left(\sqrt{(n_2 + m)!/n_2!} \tau \right), \quad (\text{A7c})$$

$$y_4(\tau) = -i \cos \theta \sin \phi_1 \sin \phi_2 \sin \left(\sqrt{n_2!/(n_2 - m)!} \tau \right), \quad (\text{A7d})$$

while the z coefficients are

$$z_1(\tau) = \cos \theta \cos \phi_1 \cos \left(\sqrt{n_3!/(n_3 - m)!} \tau \right), \quad (\text{A8a})$$

$$z_2(\tau) = \sin \theta \cos \phi_1 \cos \left(\sqrt{(n_3 + m)!/n_3!} \tau \right), \quad (\text{A8b})$$

$$z_3(\tau) = -i \sin \theta \cos \phi_1 \sin \left(\sqrt{(n_3 + m)!/n_3!} \tau \right), \quad (\text{A8c})$$

$$z_4(\tau) = -i \cos \theta \cos \phi_1 \sin \left(\sqrt{n_3!/(n_3 - m)!} \tau \right). \quad (\text{A8d})$$

Proceeding with the probabilistic approach, we perform a projective measurement on the qubit. Conditional on detecting the qubit in the excited state $|e\rangle$, the resulting unnormalized oscillator state can be obtained. As in previous cases, a local phase correction is required to eliminate residual imaginary phases (e.g., negative i factors) and recover the desired superposition. After applying this correction, the unnormalized oscillator state becomes

$$\begin{aligned} |\psi'_o(\tau)\rangle_e = & x_2(\tau) |n_1\rangle + x'_4(\tau) |n_1 - m\rangle + y_2(\tau) |n_2\rangle \\ & + y'_4(\tau) |n_2 - m\rangle + z_2(\tau) |n_3\rangle + z'_4(\tau) |n_3 - m\rangle. \end{aligned} \quad (\text{A9})$$

where $w'_4(\tau) = iw_4(\tau)$ with $w = x, y, z$. The normalization factor is simply given by

$$\mathcal{N} = [x_2^2 + x_4'^2 + y_2^2 + y_4'^2 + z_2^2 + z_4'^2]^{-\frac{1}{2}}. \quad (\text{A10})$$

We now choose appropriate values of the parameters n_1, n_2, n_3 , and m to realize the desired superpositions of four Fock states. For instance, one of the target states we aim to generate is

$$|\bar{0}\rangle_{5,1} = \frac{1}{4\sqrt{2}} (|0\rangle + \sqrt{15}|4\rangle + \sqrt{15}|8\rangle + |12\rangle). \quad (\text{A11})$$

One way to achieve this is by selecting $n_1 = m = 4, n_2 = 8, n_3 = 12$ in Eq. (A9), leading to the following explicit form for the oscillator state

$$|\phi\rangle = \mathcal{N} (C_0 |0\rangle + C_4 |4\rangle + C_8 |8\rangle + C_{12} |12\rangle), \quad (\text{A12})$$

where

$$\begin{aligned} C_0 = & \cos \theta \sin \phi_1 \cos \phi_2 \sin \left(\sqrt{4!} \tau \right), \\ C_4 = & \sin \theta \sin \phi_1 \cos \phi_2 \cos \left(\sqrt{8!/4!} \tau \right) \\ & + \cos \theta \sin \phi_1 \sin \phi_2 \sin \left(\sqrt{8!/4!} \tau \right), \end{aligned} \quad (\text{A13})$$

$$\begin{aligned} C_8 = & \sin \theta \sin \phi_1 \sin \phi_2 \cos \left(\sqrt{12!/8!} \tau \right) \\ & + \cos \theta \cos \phi_1 \sin \left(\sqrt{12!/8!} \tau \right), \end{aligned} \quad (\text{A14})$$

$$C_{12} = \sin \theta \cos \phi_1 \cos \left(\sqrt{16!/12!} \tau \right), \quad (\text{A15})$$

and the normalization factor is given by

$$\mathcal{N} = [C_0^2 + C_4^2 + C_8^2 + C_{12}^2]^{-\frac{1}{2}}. \quad (\text{A16})$$

The fidelity between the state $|\phi\rangle$ and the target binomial codeword $|\bar{0}\rangle_{5,1}$ is given by

$$F = \frac{\mathcal{N}^2}{32} \left| C_0 + \sqrt{15} C_4 + \sqrt{15} C_8 + C_{12} \right|^2. \quad (\text{A17})$$

As in previous cases, achieving unit fidelity requires numerical optimization over the parameter θ, ϕ_1, ϕ_2 , and the evolution time τ . Specifically, we scanned θ, ϕ_1 ,

and ϕ_2 over the interval $[0, \pi]$ using 251 uniformly spaced points for each, and τ over $[0, 2\pi]$ with 501 points. Within this parameter space, we identified approximately 5024 parameter combinations for which the fidelity approaches unity to within a numerical precision of 10^{-4} , and six combinations that satisfy a more stringent threshold of 10^{-6} .

Appendix B: Deterministic generation of binomial code states

In the deterministic protocol, instead of performing a projective measurement on the qubit, the oscillator state is obtained by tracing out the qubit subsystem from the joint system state. This operation inevitably reduces the purity of the oscillator state due to the loss of coherence arising from qubit-oscillator entanglement.

For the state $|\Psi(\tau)\rangle$ in Eq.(6), the reduced density matrix of the oscillator, expressed in the truncated Fock basis $|n_1 - m\rangle, |n_1\rangle, |n_1 + m\rangle$, takes the form

$$\rho_o(\tau) = \begin{pmatrix} |x_4|^2 & x_2 x_4^* & x_1 x_3^* \\ x_2^* x_4 & |x_1|^2 + |x_2|^2 & 0 \\ x_1^* x_3 & 0 & |x_3|^2 \end{pmatrix}. \quad (\text{B1})$$

A particularly favorable condition for deterministic generation occurs at specific combinations of the evolution time τ and the qubit superposition angle θ for which the amplitudes $|x_1| \approx 0$ and $|x_4| \approx 0$. Under these conditions, the reduced oscillator state approximates a nearly pure state of the form

$$|\psi_o(\tau)\rangle \approx x_2(\tau) |n_1\rangle + x_4(\tau) |n_1 - m\rangle, \quad (\text{B2})$$

which can be directly mapped (up to a local unitary transformation on the oscillator) to a binomial codeword comprising a superposition of two Fock states by selecting appropriate values of n_1 and m , analogous to the probabilistic protocol. The task then reduces to identifying specific pairs of τ and θ that, under the constraint $|x_1(\tau)| \approx 0$ and $|x_4(\tau)| \approx 0$, yield the desired superposition with high fidelity.

Table I. Optimal values of the parameters θ_{opt} and τ_{opt} at which each corresponding binomial code state achieves maximum fidelity in the deterministic generation protocol.

State	θ_{opt}	τ_{opt}	Max. Fidelity
$ \bar{0}\rangle_{1,1}$	2.356194	3.524866	0.998582
$ \bar{0}\rangle_{2,1}$	1.049291	5.441238	0.999613
$ \bar{1}\rangle_{2,1}$	2.620088	3.229557	0.999473
$ \bar{0}\rangle_{3,1}$	2.356194	3.229557	0.999052
$ \bar{0}\rangle_{2,2}$	2.092300	4.856902	0.999700
$ \bar{1}\rangle_{2,2}$	0.521504	0.772831	0.999763

This constraint fundamentally distinguishes the deterministic protocol from its probabilistic counterpart. In

Table II. Optimal values of the parameters $\theta_{\text{opt}}, \phi_{\text{opt}}$, and τ_{opt} at which each corresponding binomial code state achieves maximum fidelity in the deterministic generation protocol.

State	θ_{opt}	ϕ_{opt}	τ_{opt}	Max. Fidelity
$ \bar{0}\rangle_{3,1}$	0.314159	1.897522	4.787787	0.991509
$ \bar{0}\rangle_{4,1}$	0.502655	1.771858	6.170088	0.978205
$ \bar{1}\rangle_{4,1}$	2.965663	0.967611	5.554336	0.987996
$ \bar{1}\rangle_{5,1}$	2.827433	1.244071	5.554336	0.950207

the probabilistic approach, τ and θ are unconstrained and can be freely optimized to maximize the fidelity, allowing for a broader parameter search space. In contrast, the deterministic method limits the viable parameter sets, which inevitably reduces the achievable fidelity due to this restricted optimization landscape (see Fig. 6). This trade-off is clearly manifested in our numerical analysis, where no combination of (τ, θ) was found to yield unit fidelity (within a numerical threshold of 10^{-4}) for any of the six representative code states. The highest fidelities achieved in each case, along with the corresponding optimal parameter values, are summarized in Table I. It is important to note that these results pertain to the idealized, closed-system implementation of the deterministic protocol and do not include the effects of system–environment interactions. As expected, numerical simulations confirm that the inclusion of such interactions leads to a further degradation in fidelity.

Continuing to the case of three-component Fock superpositions, we proceed by setting $n_2 = n_1 + m$ in Eq. (18), which yields the following, leading to the bipartite state

$$\begin{aligned} |\Psi(\tau)\rangle = & x_1 |g, n_1\rangle + (x_2 + y_4) |e, n_1\rangle \\ & + (x_3 + y_1) |g, n_1 + m\rangle + y_2 |e, n_1 + m\rangle \\ & + x_4 |e, n_1 - m\rangle + y_3 |g, n_1 + 2m\rangle. \end{aligned} \quad (\text{B3})$$

After tracing out the qubit subsystem from $|\Psi(\tau)\rangle$ in Eq.(18), the reduced density matrix of the oscillator $\rho_o(\tau)$, can be expressed in the truncated Fock basis $|n_1 - m\rangle, |n_1\rangle, |n_1 + m\rangle, |n_1 + 2m\rangle$. It is given by

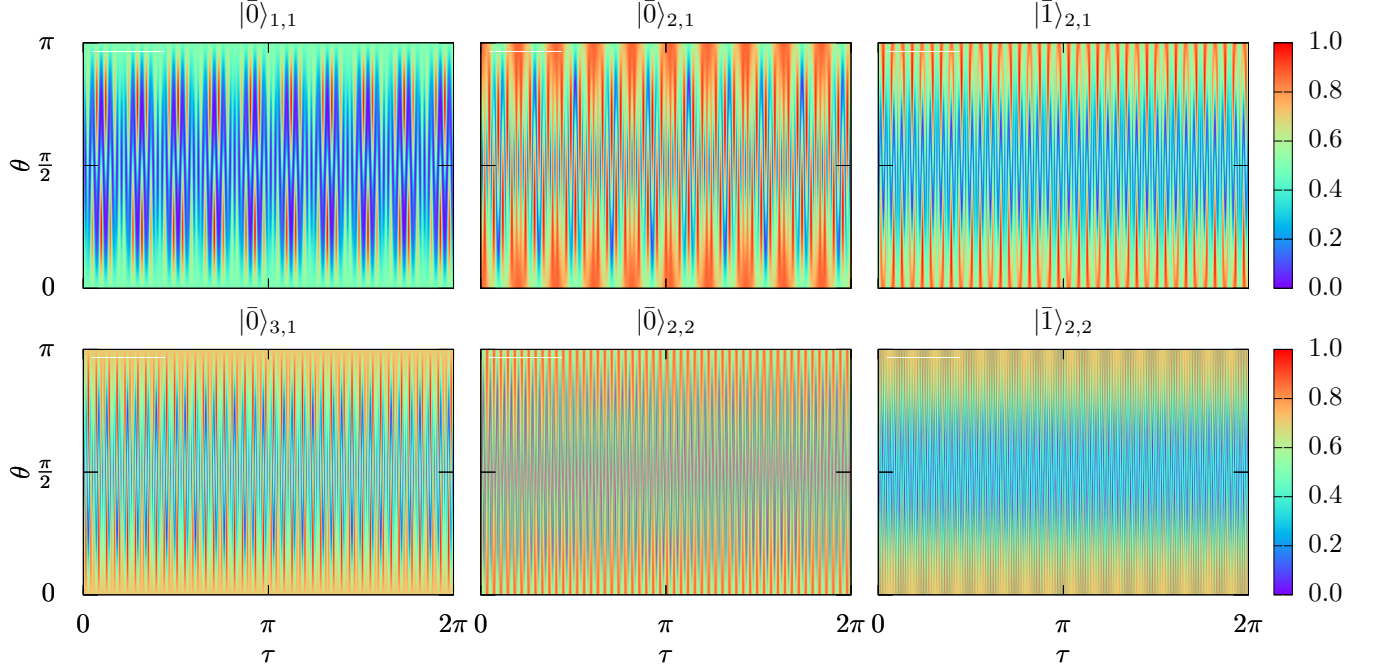


Figure 6. Fidelity between the time-evolved oscillator state $\rho_o(\tau)$ [as given in Eq. (B1)] and the corresponding target binomial codewords $|\bar{0}\rangle_{1,1}$, $|\bar{0}\rangle_{2,1}$, $|\bar{1}\rangle_{2,1}$, $|\bar{0}\rangle_{3,1}$, $|\bar{0}\rangle_{2,2}$, and $|\bar{1}\rangle_{2,2}$, plotted as a function of the evolution time τ and the qubit superposition angle θ . In contrast to the probabilistic protocol, no pair of (τ, θ) achieves unit fidelity within a numerical tolerance of 10^{-4} , highlighting the constrained parameter space inherent in the deterministic generation scheme (see main text).

$$\rho_o(\tau) = \begin{pmatrix} |x_4|^2 & (x_2 + y_4)x_4^* & x_4^*y_2 & 0 \\ (x_2^* + y_4^*)x_4 & |x_1|^2 + |x_2 + y_4|^2 & x_1^*(x_3 + y_1) + (x_2^* + y_4^*)y_2 & x_1y_3^* \\ x_4^*y_2 & x_1(x_3^* + y_1^*) + (x_2 + y_4)y_2^* & |x_3 + y_1|^2 + |y_2|^2 & (x_3^* + y_1^*)y_3 \\ 0 & x_1^*y_3 & (x_3^* + y_1^*)y_3 & |y_3|^2 \end{pmatrix}. \quad (\text{B4})$$

Now, in the limit, $x_1 \approx 0$, $x_3 \approx 0$, $y_1(\tau) \approx 0$, $y_3(\tau) \approx 0$, the above density matrix assumes the following pure state of the form

$$|\psi_o(\tau)\rangle \approx x_4 |n_1 - m\rangle + (x_2 + y_4) |n_1\rangle + y_2 |n_1 + m\rangle. \quad (\text{B5})$$

As before, this state can be mapped (up to a local unitary transformation on the oscillator) to a binomial codeword comprising a superposition of three Fock states by appropriately choosing the values of n_1 and m . However, due to constraints on the coefficients, it is not possible to attain near-unity fidelity for the desired code states. Representative best-case scenarios for the four states considered in this study are summarized in Table II.

Appendix C: Binomial codewords via rotation of primitive states

Following the framework developed in Ref. [14], in this Section, we demonstrate explicitly how the logical bino-

mial codewords defined in Eq. (1) can be obtained from a single *primitive state* using parity-selective rotations. This construction places the binomial code within the broader class of rotation-symmetric bosonic codes (RS-BCs) and highlights the underlying discrete rotational symmetries that structure these codes.

1. Construction of binomial codewords from a primitive state

We define the primitive state as a weighted superposition over Fock states spaced by $(S + 1)$, with weights drawn from binomial coefficients

$$|\Theta\rangle_{N,S} = \frac{1}{\sqrt{2^N}} \sum_{m=0}^{N+1} \sqrt{\binom{N+1}{m}} |(S+1)m\rangle. \quad (\text{C1})$$

This state includes all Fock components required to build both logical codewords $|\bar{0}\rangle_{N,S}$ and $|\bar{1}\rangle_{N,S}$, since it contains both even and odd values of m .

To extract the individual logical codewords, we exploit the discrete rotation symmetry in Fock space using the operator

$$\hat{R}(\phi) = e^{i\phi\hat{n}}, \quad \hat{n} = \hat{a}^\dagger\hat{a}. \quad (\text{C2})$$

In particular, a rotation by $\phi = \pi$ maps each Fock state as $\hat{R}(\pi)|n\rangle = (-1)^n|n\rangle$, thus separating the primitive state into parity components.

Define the logical codewords as

$$|\bar{0}\rangle_{N,S} = \mathcal{N}_0 \left(|\Theta\rangle_{N,S} + \hat{R}(\pi) |\Theta\rangle_{N,S} \right), \quad (\text{C3})$$

$$|\bar{1}\rangle_{N,S} = \mathcal{N}_1 \left(|\Theta\rangle_{N,S} - \hat{R}(\pi) |\Theta\rangle_{N,S} \right), \quad (\text{C4})$$

where \mathcal{N}_μ are normalization constants. These operations project onto even and odd values of m , respectively, thereby isolating the desired logical basis states $\mu = 0, 1$.

This construction guarantees orthogonality of the logical states and yields the exact codeword forms prescribed by the binomial code definition.

2. Example: Binomial Code for $N = 2, S = 2$

As an illustrative example, consider the case where $N = 2$ and $S = 2$, leading to Fock spacings of $(S + 1) = 3$. As defined in Eq. (3), the binomial codewords are: $|\bar{0}\rangle_{2,2} = \frac{1}{2}(|0\rangle + \sqrt{3}|6\rangle)$, $|\bar{1}\rangle_{2,2} = \frac{1}{2}(\sqrt{3}|3\rangle + |9\rangle)$. The associated primitive state is:

$$|\Theta\rangle_{2,2} = \frac{1}{2}(|0\rangle + \sqrt{3}|3\rangle + \sqrt{3}|6\rangle + |9\rangle). \quad (\text{C5})$$

Applying the parity-selective rotation $\hat{R}(\pi)$, we obtain

$$\hat{R}(\pi) |\Theta\rangle_{2,2} = \frac{1}{2}(|0\rangle - \sqrt{3}|3\rangle + \sqrt{3}|6\rangle - |9\rangle). \quad (\text{C6})$$

Therefore, it is straightforward to extract the logical

states as shown below

$$|\bar{0}\rangle_{2,2} = \frac{1}{\sqrt{4}} \left(|\Theta\rangle_{2,2} + \hat{R}(\pi) |\Theta\rangle_{2,2} \right) = \frac{1}{2} (|0\rangle + \sqrt{3}|6\rangle), \quad (\text{C7})$$

$$|\bar{1}\rangle_{2,2} = \frac{1}{\sqrt{4}} \left(|\Theta\rangle_{2,2} - \hat{R}(\pi) |\Theta\rangle_{2,2} \right) = \frac{1}{2} (\sqrt{3}|3\rangle + |9\rangle). \quad (\text{C8})$$

This confirms the validity of the rotational construction and demonstrates a clear, experimentally feasible path to generating binomial codewords from a single resource state.

3. Practical considerations

The rotation-based construction of binomial codewords from a primitive state provides a unified and elegant theoretical framework, highlighting the symmetry underlying these codes. However, from an experimental perspective, this approach does not necessarily reduce the complexity of state preparation. The primitive states $|\Theta\rangle_{N,S}$ involve superpositions over all relevant Fock states $(S+1)m$ for $m = 0, \dots, N+1$, whereas the binomial codewords occupy only a parity-restricted subset of this space.

Preparing such primitive states requires coherent control over a larger number of Fock components, increasing the sensitivity to decoherence and operational infidelity. Although in principle these states can be generated using the same multiphoton Jaynes–Cummings interactions that are used to synthesize binomial codewords directly, doing so may be less efficient: if one already has access to controlled multiphoton interactions, generating the final codewords directly is typically more practical than preparing an intermediate superposition followed by rotation-based projections.

It is worth contrasting this with the family of cat codes, where the primitive state is a coherent state—a state that is straightforward to prepare experimentally with high fidelity. For cat codes, generating the entire family through rotations of this easily accessible primitive state is both conceptually elegant and experimentally practical [69]. In contrast, the more complex primitive states required for binomial codes limit the practical advantage of the rotational construction in actual implementations.

Thus, while the rotational construction offers valuable conceptual insight, it does not intrinsically simplify the experimental path to realizing binomial code states.

-
- [1] M. A. Nielsen and I. L. Chuang, *Quantum Computation and Quantum Information: 10th Anniversary Edition* (Cambridge University Press, 2010).
 [2] S. J. Devitt, W. J. Munro, and K. Nemoto, *Rep. Prog. Phys.* **76**, 076001 (2013).

- [3] B. M. Terhal, *Rev. Mod. Phys.* **87**, 307 (2015).
 [4] J. Roffe, *Contemp. Phys.* **60**, 226 (2019).
 [5] A. Cho, *Science* **10**, 7332 (2020).
 [6] S. L. Braunstein and P. van Loock, *Rev. Mod. Phys.* **77**, 513 (2005).

- [7] C. Weedbrook, S. Pirandola, R. García-Patrón, N. J. Cerf, T. C. Ralph, J. H. Shapiro, and S. Lloyd, *Rev. Mod. Phys.* **84**, 621 (2012).
- [8] A. Serafini, *Quantum Continuous Variables* (CRC Press, 2017).
- [9] S. L. Braunstein, *Phys. Rev. Lett.* **80**, 4084 (1998).
- [10] V. V. Albert, K. Noh, K. Duivenvoorden, D. J. Young, R. T. Brierley, P. Reinhold, C. Vuillot, L. Li, C. Shen, S. M. Girvin, B. M. Terhal, and L. Jiang, *Phys. Rev. A* **97**, 032346 (2018).
- [11] C. Flühmann, T. L. Nguyen, M. Marinelli, V. Negnevitsky, K. Mehta, and J. P. Home, *Nature* **566**, 513 (2019).
- [12] L. Hu, Y. Ma, W. Cai, X. Mu, Y. Xu, W. Wang, Y. Wu, H. Wang, Y. P. Song, C. L. Zou, S. M. Girvin, L.-M. Duan, and L. Sun, *Nat. Phys.* **15**, 503 (2019).
- [13] B. M. Terhal, J. Conrad, and C. Vuillot, *Quantum Sci. Technol.* **5**, 043001 (2020).
- [14] A. L. Grimsmo, J. Combes, and B. Q. Baragiola, *Phys. Rev. X* **10**, 011058 (2020).
- [15] W. Cai, Y. Ma, W. Wang, C.-L. Zou, and L. Sun, *Fundamental Research* **1**, 50 (2021).
- [16] A. Joshi, K. Noh, and Y. Y. Gao, *Quantum Sci. Technol.* **6**, 033001 (2021).
- [17] W.-L. Ma, S. Puri, R. J. Schoelkopf, M. H. Devoret, S. Girvin, and L. Jiang, *Science Bulletin* **66**, 1789 (2021).
- [18] B. de Neeve, T.-L. Nguyen, T. Behrle, and J. P. Home, *Nat. Phys.* **18**, 296 (2022).
- [19] Z. Wang, T. Rajabzadeh, N. Lee, and A. H. Safavi-Naeini, *PRX Quantum* **3**, 020302 (2022).
- [20] V. V. Sivak, A. Eickbusch, B. Royer, S. Singh, I. Tsioutsios, S. Ganjam, A. Miano, B. L. Brock, A. Z. Ding, L. Frunzio, S. M. Girvin, R. J. Schoelkopf, and M. H. Devoret, *Nature* **616**, 50 (2023).
- [21] A. J. Brady, A. Eickbusch, S. Singh, J. Wu, and Q. Zhuang, *Prog. Quantum Electron.* **93**, 100496 (2024).
- [22] Y. Xu, Y. Wang, C. Vuillot, and V. V. Albert, “Letting the tiger out of its cage: bosonic coding without concatenation,” (2024), arXiv:2411.09668 [quant-ph].
- [23] D. Gottesman, A. Kitaev, and J. Preskill, *Phys. Rev. A* **64**, 012310 (2001).
- [24] K. Noh, V. V. Albert, and L. Jiang, *IEEE Trans. Inf. Theory* **65**, 2563 (2019).
- [25] B. Q. Baragiola, G. Pantaleoni, R. N. Alexander, A. Karanjai, and N. C. Menicucci, *Phys. Rev. Lett.* **123**, 200502 (2019).
- [26] K. Noh and C. Chamberland, *Phys. Rev. A* **101**, 012316 (2020).
- [27] K. Noh, C. Chamberland, and F. G. Brandão, *PRX Quantum* **3**, 010315 (2022).
- [28] J. Conrad, *The fabulous world of GKP codes*, *Dissertation* (2024).
- [29] P. T. Cochrane, G. J. Milburn, and W. J. Munro, *Phys. Rev. A* **59**, 2631 (1999).
- [30] Z. Leghtas, G. Kirchmair, B. Vlastakis, R. J. Schoelkopf, M. H. Devoret, and M. Mirrahimi, *Phys. Rev. Lett.* **111**, 120501 (2013).
- [31] M. Mirrahimi, Z. Leghtas, V. V. Albert, S. Touzard, R. J. Schoelkopf, L. Jiang, and M. H. Devoret, *New J. Phys.* **16**, 045014 (2014).
- [32] M. Bergmann and P. van Loock, *Phys. Rev. A* **94**, 042332 (2016).
- [33] L. Li, C.-L. Zou, V. V. Albert, S. Muralidharan, S. M. Girvin, and L. Jiang, *Phys. Rev. Lett.* **119**, 030502 (2017).
- [34] C. Chamberland, K. Noh, P. Arrangoiz-Arriola, E. T. Campbell, C. T. Hann, J. Iverson, H. Putterman, T. C. Bohdanowicz, S. T. Flammia, A. Keller, G. Refael, J. Preskill, L. Jiang, A. H. Safavi-Naeini, O. Painter, and F. G. Brandão, *PRX Quantum* **3**, 010329 (2022).
- [35] N. Ofek, A. Petrenko, R. Heeres, P. Reinhold, Z. Leghtas, B. Vlastakis, Y. Liu, L. Frunzio, S. M. Girvin, L. Jiang, M. Mirrahimi, M. H. Devoret, and R. J. Schoelkopf, *Nature* **536**, 441 (2016).
- [36] R. W. Heeres, P. Reinhold, N. Ofek, L. Frunzio, L. Jiang, M. H. Devoret, and R. J. Schoelkopf, *Nat. Commun.* **8**, 94 (2017).
- [37] P. Campagne-Ibarcq, A. Eickbusch, S. Touzard, E. Zalts-Geller, N. E. Frattini, V. V. Sivak, P. Reinhold, S. Puri, S. Shankar, R. J. Schoelkopf, L. Frunzio, M. Mirrahimi, and M. H. Devoret, *Nature* **584**, 368 (2020).
- [38] R. Dahan, G. Baranes, A. Gorlach, R. Ruimy, N. Rivera, and I. Kammer, *Phys. Rev. X* **13**, 031001 (2023).
- [39] S. Konno, W. Asavanant, F. Hanamura, H. Nagayoshi, K. Fukui, A. Sakaguchi, R. Ide, F. China, M. Yabuno, S. Miki, H. Terai, K. Takase, M. Endo, P. Marek, R. Filip, P. van Loock, and A. Furusawa, *Science* **383**, 289 (2024).
- [40] Y.-R. Chen, H.-Y. Hsieh, J. Ning, H.-C. Wu, H. L. Chen, Z.-H. Shi, P. Yang, O. Steuernagel, C.-M. Wu, and R.-K. Lee, *Phys. Rev. A* **110**, 023703 (2024).
- [41] R. Blatt and D. Wineland, *Nature* **453**, 1008 (2008).
- [42] D. Stoler, B. Saleh, and M. T. and, *Opt. Acta* **32**, 345 (1985).
- [43] M. H. Michael, M. Silveri, R. T. Brierley, V. V. Albert, J. Salmilehto, L. Jiang, and S. M. Girvin, *Phys. Rev. X* **6**, 031006 (2016).
- [44] Y.-H. Chen, W. Qin, R. Stassi, X. Wang, and F. Nori, *Phys. Rev. Res.* **3**, 033275 (2021).
- [45] E. A. Wollack, A. Y. Cleland, R. G. Gruenke, Z. Wang, P. Arrangoiz-Arriola, and A. H. Safavi-Naeini, *Nature* **604**, 463 (2022).
- [46] Y.-H. Kang, J. Song, and Y. Xia, *Opt. Lett.* **47**, 4099 (2022).
- [47] Z. Ni, S. Li, X. Deng, Y. Cai, L. Zhang, W. Wang, Z.-B. Yang, H. Yu, F. Yan, S. Liu, C.-L. Zou, L. Sun, S.-B. Zheng, Y. Xu, and D. Yu, *Nature* **616**, 56 (2023).
- [48] J. Soule, A. C. Doherty, and A. L. Grimsmo, “Concatenating binomial codes with the planar code,” (2024), arXiv:2312.14390 [quant-ph].
- [49] P.-Z. Li, W. J. Munro, K. Nemoto, and N. Lo Piparo, *Quantum Sci. Technol.* **10**, 025057 (2025).
- [50] E.-J. Chang, “High-rate extended binomial codes for multi-qubit encoding,” (2025), arXiv:2501.07093 [quant-ph].
- [51] A. Udupa, T. Hillmann, R. G. Ahmed, A. Smirne, and G. Ferrini, “Performance of rotation-symmetric bosonic codes in the presence of random telegraph noise,” (2025), arXiv:2505.08670 [quant-ph].
- [52] Y. Tanaka, Y. Mori, Y. Shingu, A. Yamaguchi, T. Yamamoto, and Y. Matsuzaki, “Single-qubit rotations on a binomial code without ancillary qubits,” (2024), arXiv:2408.12968 [quant-ph].
- [53] S. S. Chelluri, S. Sharma, F. Schmidt, S. V. Kusminskiy, and P. van Loock, “Bosonic quantum error correction with microwave cavities for quantum repeaters,” (2025), arXiv:2503.21569 [quant-ph].
- [54] J. Huang, T. J. DiNapoli, G. Rockwood, M. Yuan, P. Narasimhan, E. Gupta, M. Bal, F. Crisa, S. Garattoni, Y. Lu, L. Jiang, and S. Chakram, “Fast sideband

- control of a weakly coupled multimode bosonic memory,” (2025), [arXiv:2503.10623 \[quant-ph\]](#).
- [55] C. Sukumar and B. Buck, *Phys. Lett. A* **83**, 211 (1981).
 - [56] S. Singh, *Phys. Rev. A* **25**, 3206 (1982).
 - [57] A. Shumovsky, F. L. Kien, and E. Aliskenderov, *Phys. Lett. A* **124**, 351 (1987).
 - [58] F. L. Kien, M. Kozierowski, and T. Quang, *Phys. Rev. A* **38**, 263 (1988).
 - [59] W. Vogel and D.-G. Welsch, *Phys. Rev. A* **40**, 7113 (1989).
 - [60] C. J. Villas-Boas and D. Z. Rossatto, *Phys. Rev. Lett.* **122**, 123604 (2019).
 - [61] R. Puebla, G. Zicari, I. Arrazola, E. Solano, M. Paternostro, and J. Casanova, *Symmetry* **11**, 695 (2019).
 - [62] T. K. Mavrogordatos, *Phys. Rev. A* **104**, 063717 (2021).
 - [63] P. Laha, P. A. A. Yasir, and P. van Loock, *Phys. Rev. Res.* **6**, 033302 (2024).
 - [64] P. Laha, P. A. A. Yasir, and P. van Loock, *Phys. Rev. A* **111**, 013710 (2025).
 - [65] F. W. Strauch, K. Jacobs, and R. W. Simmonds, *Phys. Rev. Lett.* **105**, 050501 (2010).
 - [66] S. Felicetti, D. Z. Rossatto, E. Rico, E. Solano, and P. Forn-Díaz, *Phys. Rev. A* **97**, 013851 (2018).
 - [67] D. Leibfried, R. Blatt, C. Monroe, and D. Wineland, *Rev. Mod. Phys.* **75**, 281 (2003).
 - [68] H. Häffner, C. Roos, and R. Blatt, *Phys. Rep.* **469**, 155 (2008).
 - [69] P.-Z. Li and P. van Loock, *Adv. Quantum Technol.* **6**, 2200151 (2023).
 - [70] D. M. Meekhof, C. Monroe, B. E. King, W. M. Itano, and D. J. Wineland, *Phys. Rev. Lett.* **76**, 1796 (1996).
 - [71] M. Hofheinz, E. M. Weig, M. Ansmann, R. C. Bialczak, E. Lucero, M. Neeley, A. D. O’Connell, H. Wang, J. M. Martinis, and A. N. Cleland, *Nature* **454**, 310 (2008).
 - [72] Y. Chu, P. Kharel, T. Yoon, L. Frunzio, P. T. Rakich, and R. J. Schoelkopf, *Nature* **563**, 666 (2018).
 - [73] F. Wolf, C. Shi, J. C. Heip, M. Gessner, L. Pezzè, A. Smerzi, M. Schulte, K. Hammerer, and P. O. Schmidt, *Nat. Commun.* **10**, 2929 (2019).
 - [74] U. von Lüpke, Y. Yang, M. Bild, L. Michaud, M. Fadel, and Y. Chu, *Nat. Phys.* **18**, 794 (2022).
 - [75] S. Li, Z. Ni, L. Zhang, Y. Cai, J. Mai, S. Wen, P. Zheng, X. Deng, S. Liu, Y. Xu, and D. Yu, *Phys. Rev. Lett.* **132**, 203602 (2024).
 - [76] X. Deng, S. Li, Z.-J. Chen, Z. Ni, Y. Cai, J. Mai, L. Zhang, P. Zheng, H. Yu, C.-L. Zou, S. Liu, F. Yan, Y. Xu, and D. Yu, *Nature Physics* **20**, 1874 (2024).
 - [77] Q. R. Rahman, I. Kladarić, M.-E. Kern, L. c. v. Lachman, Y. Chu, R. Filip, and M. Fadel, *Phys. Rev. Lett.* **134**, 180801 (2025).
 - [78] P. Laha, D. W. Moore, and R. Filip, *Adv. Quantum Technol.* **6**, 2300168 (2023).
 - [79] S. Endo, Y. Suzuki, K. Tsubouchi, R. Asaoka, K. Yamamoto, Y. Matsuzaki, and Y. Tokunaga, “Quantum error mitigation for rotation symmetric bosonic codes with symmetry expansion,” (2022), [arXiv:2211.06164 \[quant-ph\]](#).
 - [80] E. Jaynes and F. Cummings, *Proc. IEEE* **51**, 89 (1963).
 - [81] B. W. Shore and P. L. Knight, *J. Mod. Opt.* **40**, 1195 (1993).
 - [82] J. Larson and T. Mavrogordatos, *The Jaynes–Cummings Model and Its Descendants*, 2053-2563 (IOP Publishing, 2021).
 - [83] L. Li, D. J. Young, V. V. Albert, K. Noh, C.-L. Zou, and L. Jiang, *Phys. Rev. A* **103**, 062427 (2021).
 - [84] P.-Z. Li, J. Dias, W. J. Munro, P. van Loock, K. Nemoto, and N. Lo Piparo, *Adv. Quantum Technol.* **7**, 2300252 (2024).
 - [85] Y.-x. Liu, L. F. Wei, and F. Nori, *Phys. Rev. A* **71**, 063820 (2005).
 - [86] D. S. Schlegel, F. Minganti, and V. Savona, *Phys. Rev. A* **106**, 022431 (2022).
 - [87] P. Laha, L. Slodička, D. W. Moore, and R. Filip, *Opt. Express* **30**, 8814 (2022).
 - [88] P. Laha, *J. Opt. Soc. Am. B* **40**, 1911 (2023).
 - [89] P. Laha, D. W. Moore, and R. Filip, *Phys. Rev. Lett.* **132**, 210201 (2024).